Determination of fluid and gel domain sizes in two-component, two-phase lipid bilayers

An electron spin resonance spin label study

M. B. Sankaram,* D. Marsh,‡ and T. E. Thompson*

*Department of Biochemistry, University of Virginia Health Sciences Center, Charlottesville, Virginia 22908 USA; and ‡Abteilung Spektroskopie, Max-Planck-Institut für Biophysikalische Chemie, WD-3400 Göttingen, Federal Republic of Germany

ABSTRACT The average sizes of fluid and gel domains in the two-component, two-phase system formed from mixtures of dimyristoyl phosphatidylcholine and distearoyl phosphatidylcholine were determined from an analysis of the electron spin resonance spectral lineshapes of a dimyristoyl phosphatidylcholine–nitroxide spin label as a function of spin label concentration. The ratio, R, of the intensities measured at two magnetic field strengths was found to be diagnostic of a statistical distribution of spin labels in disconnected domains. R is defined as $V'/2V^{pp}$, where V^{pp} is the maximum intensity and V' is the intensity at a position in the wings of a first derivative electron spin resonance line that is a constant multiple of the peak-to-peak linewidth. The intensity ratio for Gaussian or Voigt lineshapes is less than or equal to the value for a Lorentzian lineshape. The intensity ratio was found to be greater than the value for a Lorentzian line when spectra from disconnected domains containing a statistical distribution of spin labels undergoing spin–spin interactions were summed. The intensity ratio, R, calculated by spectral simulations as a function of the average number of labels per domain, N, was found to increase to a maximum with increasing N and then to decrease. The dependence on spin label concentration of the experimentally measured intensity ratios paralleled this predicted behavior. A method is presented to calculate the average number of lipids per fluid or gel domain based on a knowledge of R, and of the distribution of the spin label between the fluid and gel phases determined from the phase diagram. The results demonstrate that the number of lipids per domain increases linearly from a fixed number of nucleation sites, as the fraction of the phase that is disconnected increases. At any given mole fraction of the particular phase, the gel domains are bigger than the fluid domains because they have a lower nucleation density. The results also suggest that the disconnected domains are, in most cases, nonrandomly distributed in the plane of the bilayer.

INTRODUCTION

The protein and lipid components in many biological membranes appear to be organized into in-plane domains (1). Such domain structure can be the result of specific lipid–lipid, lipid–protein, and protein–protein interactions. In a number of biological membranes, protein-rich domains can be observed by fluorescence microscopy when the fluorescence of labeled lipids or proteins is monitored. The average size of such domains is on the order of 1,000 nm in diameter (2–4).

Domain structure in lipid monolayers formed at the air–water interface can be visualized by epifluorescence microscopy combined with surface balance techniques (5). The domains in one- and two-component lipid monolayers determined by this method are ~10,000 nm in diameter or greater (6). In two-component monotectic (7), peritectic (8), and eutectic (9) lipid bilayer systems examined in the gel–fluid coexistence region, the fluorescence photobleaching recovery method has clearly shown the existence of domains for the gel and fluid phases. Such studies have suggested that when one of the phases forms isolated domains, the other phase forms a continuous reticular structure (8).

So far, it has not been possible to observe directly by optical microscopy the gel or fluid domains formed in two-component, two-phase lipid bilayer systems (Thompson, T. E., unpublished observations) except with charged lipids and calcium. The reason for this might be that the domains in these systems are smaller than those detected so far in biological membranes and in lipid monolayers. Thus, alternative methods must be sought to determine the sizes of lipid domains in bilayers.

The aim of the present investigation is to determine the average sizes of fluid and gel domains in a peritectic lipid mixture formed from dimyristoyl phosphatidylcholine (DMPC) and distearoyl phosphatidylcholine (DSPC). The temperature–composition phase diagram for this system, which exhibits both gel–gel and gel–fluid immiscibility, is shown in Fig. 1 (10). The experimental strategy used involves the introduction of a spin-labeled phosphatidylcholine into the lipid mixture and monitoring of the electron spin resonance (ESR) spectral linewidths and lineshapes as the domain structure in the host system is changed by compositional and temperature variations (cf. Fig. 1). The method requires a diagnostic means for the analysis of unresolved ESR spectral components such as those that arise from spin-labeled lipids undergoing spin–spin interactions in disconnected phospholipid domains. The one developed here is based on a previous treatment of the conventional form of inhomogeneous spectral broadening arising from unresolved hyperfine structure (11–13).

MATERIALS AND METHODS

The phospholipids DMPC and DSPC were purchased from Avanti Polar Lipids, Inc. (Alabaster, AL). Spin-labeled dimyristoyl phosphatidylcholine (13-DMPCSL) with the spin label attached to the 13-C atom in the *sn*-2 chain was synthesized as described previously by acylation

Address correspondence to Dr. Sankaram.

0006-3495/92/08/340/10 $2.00

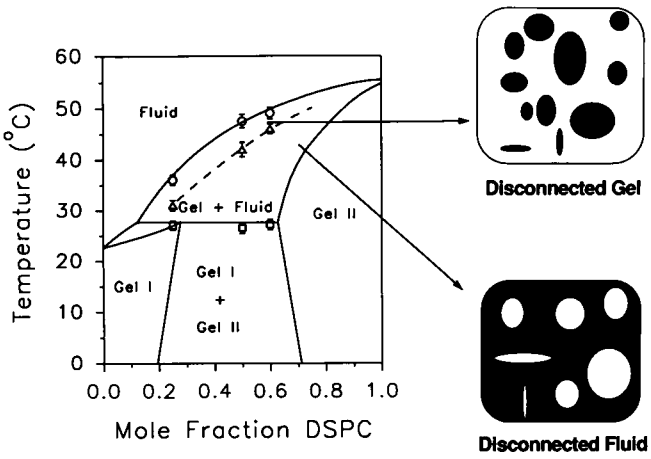

FIGURE 1 Temperature–composition phase diagram for the DMPC-DSPC system. The solid lines represent the phase boundaries determined by Knoll et al. (10). The dashed line in the gel–fluid coexistence region is the line of connectivity determined by fluorescence photobleaching experiments (8). The points of discontinuity observed in this work at the solidus (□), at the fluidus (○), and at the point of connectivity (△) within the gel–fluid coexistence region when the peak-to-peak linewidths of 13-DMPCSL are monitored as a function of temperature are also shown. A schematic representation of the disconnected fluid–connected gel and the disconnected gel–connected fluid situations encountered below and above the point of connectivity, respectively, is included. The disconnected fluid and gel domains are shown to be different in both size and shape.

of 1-myristoyl-2-lyso-*sn*-glycero-3-phosphocholine with the corresponding spin-labeled myristic acid, 13-MASL (14). The other positional isomers of spin-labeled phosphatidylcholine (*n*-PCSL) were synthesized by acylation with spin-labeled stearic acids, *n*-SASL, of lysophosphatidylcholine (derived from egg yolk lecithin) containing predominantly palmitoyl chains (14). Multilamellar vesicles were prepared by dispersing dried thin films of the lipid mixtures, containing the required concentration of spin label, in aqueous buffer (0.01 M sodium phosphate buffer, pH 7.5, containing 0.05 M KCl). The spin label concentrations were in the range 0.1–4 mol% with respect to total lipid. ESR spectra were recorded on a 9-GHz Varian Century Line series spectrometer (Varian Associates, Inc., Palo Alto, CA). Sample temperature was controlled by a thermostatted nitrogen gas flow regulation system. The sealed sample capillaries of 1 mm outer diameter were placed in a quartz tube containing silicone oil for thermal stability. An IBM PC was used for digital data collection using software written by Dr. M. D. King (Max-Planck-Institut für Biophysikalische Chemie, Göttingen).

THEORETICAL LINESHAPE ANALYSIS

When spin-labeled lipids are present in a lipid mixture that exhibits lateral phase separation, such as is depicted in Fig. 1, the various disconnected domains will contain statistically different concentrations of spin labels. A pictorial illustration for the shape and size heterogeneity expected for in-plane gel and fluid domains is shown in the right panel of Fig. 1. The disconnected domains are treated in this analysis in terms of an average size. For the moment, the spin labels present in the connected phase are neglected (but see below). If the spin labels are in slow exchange between domains on the ESR timescale, the ESR spectrum will consist of a superposition of spectral lines from the individual domains which have different degrees of spin–spin broadening. The resulting composite spectrum will then be a single inhomogeneously broadened line in which the inhomogeneity arises from a distribution of linewidths rather than from a distribution of line positions (which is the case normally considered). The effects of this different type of inhomogeneous broadening on the spectral lineshapes are analyzed here by using a modified form of the method due originally to Bales (11–13).

The type of inhomogeneous broadening obtained when the spin labels are statistically distributed among disconnected domains is illustrated in Fig. 2. If the average number of spin labels per domain is N, the number of domains is N_{dom}, and the total number of spin labels is N_t ($=N \times N_{dom}$), the probability, P_n, of finding n spin labels in a domain is given by a binomial distribution function:

$$P_n = \frac{N_t!}{(N_t - n)!}\left[\frac{1}{N_{dom}}\right]^n\left[1 - \frac{1}{N_{dom}}\right]^{N_t - n}. \quad (1)$$

When N_{dom} and the total number of spin labels, N_t are large, Eq. 1 may be approximated by the Poisson distribution function:

$$P_n = \frac{N^n}{n!}e^{-N}. \quad (2)$$

For a particular domain, the ESR linewidth is determined by the number, n, of spin labels that are present in the domain, and is given by:

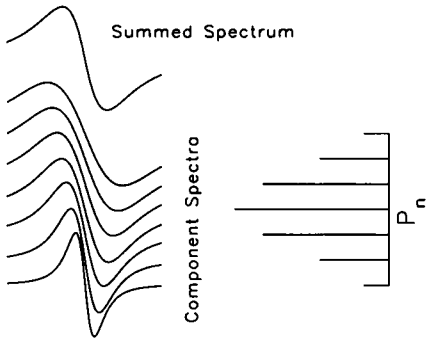

FIGURE 2 Illustration of inhomogeneous broadening of ESR lines from spin labels statistically distributed between different domains. Summation is performed over domains containing different concentrations of spin labels. Each domain gives a spectrum that has either a pure Lorentzian lineshape or a lineshape with Gaussian character arising from unresolved proton hyperfine structure. The spectra from the different domains are centered about the same position but differ in their peak-to-peak linewidths, which are proportional to the concentration of the labels in the domain. The concentration distribution is given by a binomial distribution function, indicated by the stick plot on the right. Only a selection of the component spectra used to obtain the summed spectrum is shown.

$$\Delta H^{pp} = \Delta H_0^{pp} + \frac{d\Delta H^{pp}}{dn} n. \quad (3)$$

Here ΔH_0^{pp} is the limiting linewidth at low concentration, and $d\Delta H^{pp}/dn$ is the gradient with concentration of the linewidth. ΔH_0^{pp} is usually $\sim$1 G and $d\Delta H^{pp}/dn$ is between 0.1 and 0.8 G/mol% for a number of different spin labels incorporated in fluid phase lipid bilayers (15).

The inhomogeneous broadening arising from a statistical distribution of labels between domains can be distinguished from other forms of spectral broadening (both homogeneous and inhomogeneous) by the diagnostic lineshape intensity ratio, R, which is defined in references 11–13 as:

$$R = \frac{V'}{2V^{pp}}, \quad (4)$$

where V^{pp} is the peak-to-peak amplitude of the first derivative ESR display. $V'/2$ is the height above the baseline at the diagnostic position in the spectral wings, which is defined to be $\pm 1.32\Delta H^{pp}$ distant from the central resonance position, where ΔH^{pp} is the peak-to-peak linewidth (see insert to Fig. 3, below). This intensity ratio is a property only of the lineshape and is independent of the magnitude of the spectral broadening. For a Lorentzian line, it has the value of $R^L = 0.213$ and for a Gaussian line a value of $R^G = 0.067$. Voigt lineshapes have intermediate values of R depending on the degree of Gaussian broadening arising from unresolved proton hyperfine structure. Experimental ESR spectra of lipid spin labels in gel and fluid phases of one-component lipid bilayers are described by one of these three lineshape functions, provided, as is the case here, that the spectral anisotropy can be neglected (12, 15).

When values of the intensity ratio, R, are calculated as a function of N using the model with disconnected domains described above and illustrated by the inhomogeneous broadening shown in Fig. 2, the results given in Fig. 3 are obtained. For the case in which the component spectra are all Lorentzian, the dependence of R on N is shown by the solid line. The dashed line shows the result when the component spectra have varying non-Lorentzian lineshapes, simulating unresolved proton hyperfine structure. In either case, R is seen to decrease with increasing N, when N is greater than 8. Further, it is found that when $N > 10$, the value of R is independent of the linewidths and lineshapes of the individual component lines and is also independent of ΔH_0^{pp} and $d\Delta H^{pp}/dn$. When $0 < N < 8$, R increases with increasing N. In this region, the values of R depend critically on the choice of the linewidths for the component spectra and on whether or not unresolved proton hyperfine structure is included. In this range for N, a significant number of domains contain no spin labels. Therefore, the probability distribution that determines the spectral intensity is biased to higher values of N than is the actual distribution function. This shift leads to a higher weighting for the broader spectra, resulting in increasing values of R with increasing N.

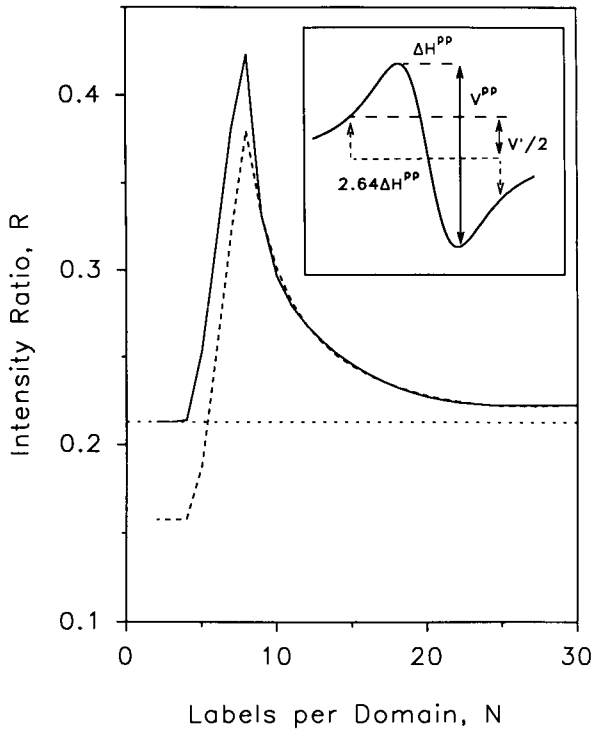

FIGURE 3 Calculated dependence of the intensity ratio, R, on the average number of spin labels per domain, N. The intensity ratios were measured from spectra obtained by adding individual Lorentzian lines of different widths. The Lorentzian linewidths were assumed to vary linearly with the number of spin labels per domain, n (cf. Eq. 3). The weighting factors for summation were obtained using a binomial distribution function (see Eq. 1) or a Poisson distribution (Eq. 2) at high values of N. The solid line was obtained when all the component spectra in domains were pure Lorentzians and therefore differed only in their linewidths but had a constant value of R. The dashed line was obtained when unresolved proton hyperfine structure was included. Each component line was composed of seven binomially distributed Lorentzian lines with an individual proton hyperfine splitting of a_H = 0.16 G (cf. reference 11). In this case, the (composite) component lines differ in both linewidth and the values of R. The horizontal dotted line is the value of R for a Lorentzian line, R^L. The spectral positions for definition of the diagnostic intensity ratio according to references 11–13 are indicated in the insert.

It is clear from Fig. 3 that the intensity ratios for composite spectral lines consisting of a summation of individual lines of different widths, but centered about the same position, are greater than the maximum value, R^L = 0.213, possible for a single spectral line or for lines corresponding to fast exchange. This is because in the latter cases the lines have either Lorentzian, Gaussian, or Voigt lineshapes. Therefore, experimental values of $R_{obs} > R^L$ are diagnostic for lineshapes arising from unresolved spectral components undergoing slow exchange and in particular for disconnected phases containing a distribution of spin labels.

In the model used to calculate the results shown in Fig.

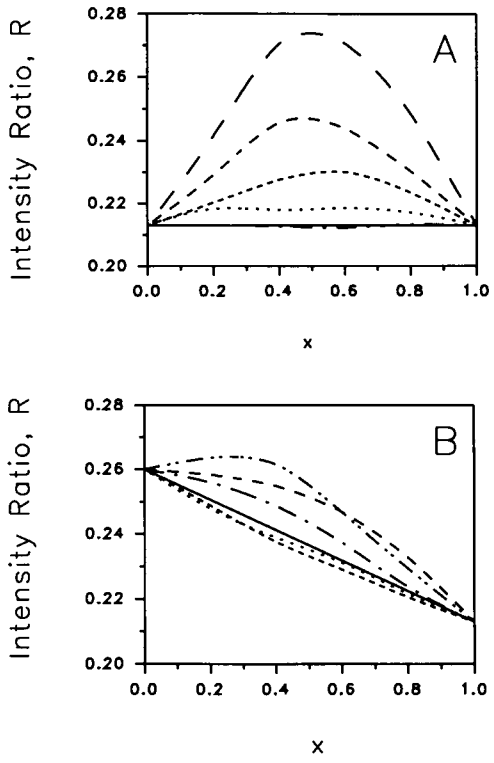

FIGURE 4 (*A*) Intensity ratios, R, measured on summed spectra for which two Lorentzians of peak-to-peak linewidths ΔH_1^{pp} and ΔH_2^{pp} are added. Values of R are plotted as a function of the fraction, x, of the Lorentzian with width ΔH_2^{pp}. The fractional difference in linewidth, $(\Delta H_2^{pp} - \Delta H_1^{pp}/\Delta H_1^{pp})$, is: 0.1 (-· ··· ·-), 0.2 (-·····-), 0.3 (· · · · · ·), 0.4 (--------), and 0.5 (– – – –). The solid line gives the weighted average values for R (cf. Eq. 5). (*B*) Intensity ratios, R, measured on summed spectra in which a Lorentzian of width ΔH_2^{pp} is added to a non-Lorentzian line of width ΔH_1^{pp} = 1.58 G with intensity ratio 0.260. The values of ΔH_2^{pp} are 0.8 G (--------), 1.2 G (· · · · · ·), 1.8 G (-·-·-·-·-), 2.0 G (– – – –), and 2.4 G (-· ··· ·-), corresponding to fractional differences in linewidth of −0.494, −0.240, 0.126, 0.266, and 0.519, respectively. The solid line shows the intensity ratios when R is a weighted average of the values for the two component lines, namely, 0.260 and 0.213 (cf. Eq. 5).

3, the spin labels are confined to the disconnected phase. However, the spin labels in the DMPC/DSPC system are actually present in both the disconnected and connected phases. The effect on the experimentally observed values of the intensity ratio, R_{obs}, of this superposition of spectra from the two phases was examined by spectral simulations in two ways. In one, two Lorentzian lines of widths ΔH_1^{pp} and ΔH_2^{pp} were summed to produce a simulated spectrum from which R was calculated as a function of the proportion, x, of the Lorentzian with width ΔH_2^{pp}. The results of this calculation are shown in Fig. 4 *A* for various values of the fractional difference in linewidth, $(\Delta H_2^{pp} - \Delta H_1^{pp})/\Delta H_1^{pp}$. When this value was >0.6, the two components were resolved in the composite spectrum. At lower values, the summed spectra had an apparent single-component lineshape for which R changed both with x and with the fractional difference in linewidth. However, up to an ~10% difference in the component linewidths, R did not change significantly from the single Lorentzian value of 0.213. In the second set of simulations, the results of which are shown in Fig. 4 *B*, a Lorentzian (R^L = 0.213) of width ΔH_2^{pp} was added to a spectrum with width ΔH_1^{pp} = 1.58 G and a value of R = 0.260. ΔH_2^{pp} was varied from 0.8 to 2.4 G. The variation of R with x and with the fractional difference in linewidth paralleled that found in Fig. 4 *A* for the two Lorentzians. When the fractional change in linewidth is less than ~0.1, it is found that R_{obs} is approximated reasonably well by a weighted average of the component R values (cf. Fig. 4 *B*):

$$R_{obs} = fR_f + (1 - f)R_g, \tag{5}$$

where R_f and R_g are the intensity ratios of the fluid and gel phase component spectra, respectively, and f is the mole fraction of the spin label in the fluid phase. It can be assumed that one of the two component intensity ratios is always a constant at R^L = 0.213 since, when one phase is disconnected, the other phase is connected (8).

The value required for the mole fraction, f, of spin-labeled lipid in the fluid phase can be obtained from the phase diagram (Fig. 1) by assuming that the spin-labeled lipid is distributed in the same way as that of the parent unlabeled lipid component. The fraction, F, of lipid in the fluid phase at mole fraction X of the parent unlabeled component is given by the lever rule (see, for example, reference 16):

$$F = \frac{X_S - X}{X_S - X_F}, \tag{6}$$

where X_S and X_F are the mole fractions of the parent unlabeled component at the solidus and fluidus boundaries of the tie line at the relevant temperature. The fraction of the parent unlabeled component (or correspondingly of spin-labeled lipid) in the fluid phase is then given simply by:

$$f = \frac{FX_F}{X}. \tag{7}$$

This value can then be used in Eq. 5 to determine the intrinsic value of R for the disconnected phase (fluid or gel) from the value, R_{obs}, that is determined experimentally.

RESULTS

ESR spectra of 13-DMPCSL

The phase separation and domain structure of DMPC-DSPC mixed bilayers have been studied from the concentration and temperature dependence of the ESR spectra of a spin-labeled analogue of one of the lipid components. The spin-labeled lipid used mostly in this work (13-DMPCSL) is a derivative of DMPC in which the paramagnetic nitroxide group is attached to the 13-C

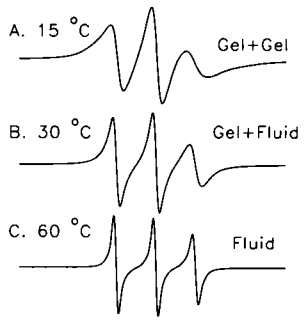

FIGURE 5 ESR spectra of 13-DMPCSL in a 50:50 (mol/mol) mixture of DMPC with DSPC. The spin label concentration is 3 mol%. (*A*) Spectrum in the gel–gel immiscible region at 15°C. (*B*) Spectrum in the gel–fluid coexistence region at 30°C. (*C*) Spectrum in the fluid phase at 60°C. Spectral width is 100 G. The three lines are referred to from left to right as the low-field, central, and high-field lines, respectively.

atom of the *sn*-2 myristoyl chain. This terminal position of labeling is likely to give rise to least perturbation of the native molecular structure and ensure that the spin-labeled lipid distributes itself in lipid mixtures in a manner similar to that of the parent unlabeled DMPC. The latter supposition is borne out by experiments on the distribution of the spin label by spontaneous transfer between vesicles of different lipid compositions (Wimley, W., and T. E. Thompson, unpublished data).

Fig. 5 shows the ESR spectra of the 13-DMPCSL spin label incorporated at a concentration of 3 mol% in an equimolar mixture of DMPC and DSPC. At the three temperatures indicated, namely, 10, 30, and 60°C, the system goes, respectively, from gel–gel phase immiscibility, through gel–fluid phase coexistence, to the fluid phase (cf. Fig. 1). With the possible exception of the gel–gel immiscibility region, the ESR spectra shown in Fig. 5 are essentially typical of a one-component system. The single-component nature of the spectra was retained when spin label derivatives of phosphatidylcholine with the nitroxide moiety attached to the 14- or the 16-position in the *sn*-2 acyl chain were used and the acyl chain composition of the spin labels was varied.

Linewidth analysis

Fig. 6 shows the dependence of the peak-to-peak linewidth, ΔH^{pp}, of the three hyperfine lines in the ESR spectra of 13-DMPCSL as a function of temperature. The data were obtained from an equimolar DMPC-DSPC mixture. The high-field line was found to be most responsive to temperature-induced changes in the lipid phase. Discontinuities in ΔH^{pp} were observed at the solidus and fluidus boundaries. In addition, a discontinuity was observed within the gel–fluid coexistence region at the temperature of the connectivity threshold (43°C for the equimolar mixture) that has been identified by fluorescence photobleaching recovery experiments (8). Similar points of discontinuity were observed as the concentration of the spin label was varied in the range 0.1–4 mol% for three DMPC-DSPC mixtures of total molar composition 75/25, 50/50, and 40/60. The points of discontinuity obtained for the three systems from the present ESR experiments are shown in Fig. 1 as open squares, open circles, and open triangles (see above).

In principle, the apparent one-component nature of the ESR spectra in the gel–fluid coexistence regions could be due to a rapid exchange of the spin label between the two phases. This possibility is analyzed here and shown to be inconsistent with the temperature dependence of the linewidths observed in the phase separation region. In the fast exchange approximation, the observed peak-to-peak linewidth is given by:

$$\Delta H^{pp} = f\Delta H_f^{pp} + (1 - f)\Delta H_g^{pp}, \quad (8)$$

where ΔH_f^{pp} is the peak-to-peak linewidth in the fluid phase, ΔH_g^{pp} is the peak-to-peak linewidth in the gel phase, and f is the fraction of the spin label in the fluid phase. The values of f are calculated from the phase diagram (Fig. 1) by application of the lever rule (see Eqs. 6 and 7), assuming that the spin label is distributed between the two phases in the same way as is the parent DMPC. ΔH_g^{pp} and ΔH_f^{pp} may be obtained at the required temperatures by extrapolation of the data from the gel

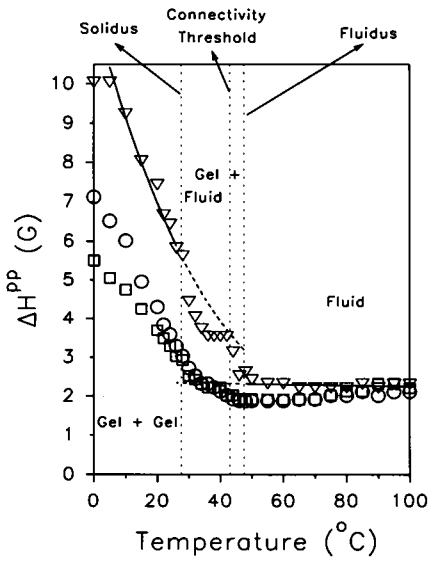

FIGURE 6 Temperature dependence of the peak-to-peak linewidths, ΔH^{pp}, of 13-DMPCSL incorporated at a concentration of 3 mol% in an equimolar mixture of DMPC and DSPC. Data from the low-field (○), central (□), and high-field (▽) hyperfine lines are included. The heavy lines are a third order polynomial fit to the gel phase data and a linear regression for the fluid phase data. The extrapolated values of the linewidth for the gel (ΔH_g^{pp}) and fluid (ΔH_f^{pp}) phases were obtained by this fitting procedure and are indicated by the dashed lines. These values were used in Eq. 8 to calculate ΔH^{pp} in the coexistence region. The vertical dotted lines indicate the solidus and fluidus phase boundaries determined from Fig. 1.

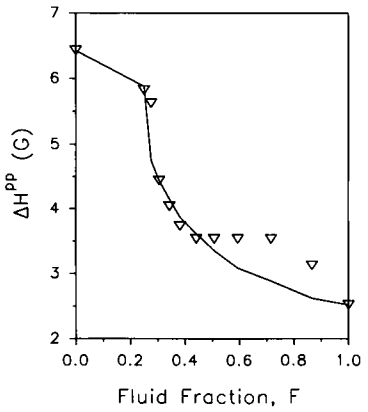

FIGURE 7 Experimental (▽) and calculated (——) peak-to-peak linewidths, ΔH^{pp}, of the high-field hyperfine line as a function of mole fraction, F, of the fluid phase. The experimental points are obtained from an equimolar mixture of DMPC and DSPC containing the spin label 13-DMPCSL at a concentration of 3 mol%. The fluid fractions at various temperatures in the coexistence region are obtained by application of the lever rule to the phase diagram shown in Fig. 1. The solid line is calculated using the fast-exchange model given by Eq. 8.

and fluid phases into the gel–fluid coexistence region, as indicated in Fig. 6.

Fig. 7 shows the experimental and calculated values of ΔH^{pp} plotted as a function of the fraction, F, of lipids in the fluid phase, which is also obtained from the phase diagram (see Eq. 6). Clearly, although the agreement between the fast exchange approximation and experiment is good below the point of connectivity, it is not good above it. We therefore conclude that the fast exchange approximation does not hold for this system.

Intensity ratio analysis

In view of the failure of the fast exchange model, it must be assumed that the alternative model holds; namely, that in the two-phase regions the spin label undergoes only slow exchange between domains on the ESR timescale. The apparent single-component nature of the ESR spectra in the coexistence region must therefore arise because the differences in hyperfine splittings of labels in the gel and fluid phases are smaller than the corresponding component linewidths. Inhomogeneous broadening of the resulting composite spectra arises from the distribution of linewidths from the different domains, which was analyzed in terms of intensity ratios, R (11–13), in the theoretical section above. This analysis is now applied to the experimental lineshapes from the 13-DMPCSL spin label in DMPC-DSPC mixtures.

The temperature dependence of the experimentally observed intensity ratio, R_{obs}, for 13-DMPCSL in an equimolar mixture of DMPC with DSPC is given in Fig. 8. In the fluid phase the intensity ratios of all three ^{14}N hyperfine lines are equal to the Lorentzian value: R^L = 0.213. This is because at 3 mol% 13-DMPCSL the unresolved proton hyperfine structure is completely exchange-narrowed, resulting in a pure Lorentzian lineshape (cf. reference 15). In the gel–fluid phase coexistence region, it is seen that $R_{obs} > R^L$ at all temperatures and for all three hyperfine lines, suggestive of the presence of disconnected domains throughout the phase separation region. In the gel phase, the values differ between the various hyperfine lines. Some of the values are greater than those for a pure Lorentzian, which may be due to the gel–gel phase separation or possibly some residual spectral anisotropy at low temperatures in the gel phase.

The dependence of the experimental intensity ratios on the spin label concentration is given in Fig. 9, again for 13-DMPCSL in an equimolar mixture of DMPC and DSPC. It is seen that R_{obs} first increases as the spin label concentration is increased, reaches a maximum, and then decreases. Qualitatively, this mirrors the dependence on the average number of spin labels per domain, N, that was predicted by the simulations given in Fig. 3. This gives further support to the method of analysis and the interpretation in terms of the existence of disconnected domains, since increasing the overall spin label concentration should result in a direct increase in the average number of spin labels per domain.

Domain sizes

The intrinsic intensity ratios, R_f and R_g, in the disconnected phases can be obtained from the measured values of R_{obs} in the two-phase region (cf. Fig. 8) by using information from the binary phase diagram in conjunction with Eqs. 5–7. These values can then be used together

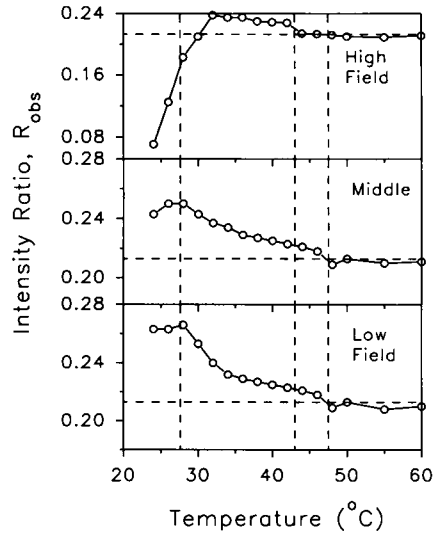

FIGURE 8 Temperature dependence of the experimental intensity ratio, R_{obs}, for the low-field, central, and high-field ESR lines of the 13-DMPCSL spin label at a concentration of 3 mol% in a 50:50 (mol/mol) mixture of DMPC with DSPC. The vertical dashed lines from left to right represent the solidus, the point of connectivity, and the fluidus phase boundary, respectively (cf. Fig. 1). The horizontal dashed line in each panel is the value of R for a pure Lorentzian line, R^L.

with the calibrations derived from spectral simulations for a statistical distribution of spin labels between the disconnected domains (Fig. 3) to obtain the average numbers, N_f and N_g, of spin labels per domain. The spin label concentrations (cf. Fig. 9) are chosen such that the values of R correspond to $N \geq 10$ in Fig. 3, for which the calibration is insensitive to the linewidth parameters and the degree of Gaussian broadening. Further, it is ensured that the data are chosen such that the linear additivity of the intensity ratios given by Eq. 5 is also valid.

The values for the average number of spin labels per fluid domain, N_f, may be related to the average domain size (i.e., the average number of lipids per fluid domain, L_f) by using parameters that may also be obtained from the phase diagram. The average density of spin labels in a domain, N_f/L_f, is given by fc/F, where c is the mole fraction of spin-labeled lipid. Therefore, the average number of lipids per fluid domain below the point of connectivity is given by:

$$L_f = \frac{N_f F}{fc}, \tag{9}$$

and correspondingly the average number of lipids per gel domain above the point of connectivity is given by:

$$L_g = \frac{N_g(1-F)}{(1-f)c}. \tag{10}$$

The required values of f and F are obtained from the binary phase diagram using Eqs. 6 and 7 given above. In particular, the relations $F/f = X/X_F$ and $(1-F)/(1-f) = X/X_S$ are used. Again it is assumed that the spin label distributes in the same way as the parent unlabeled lipid.

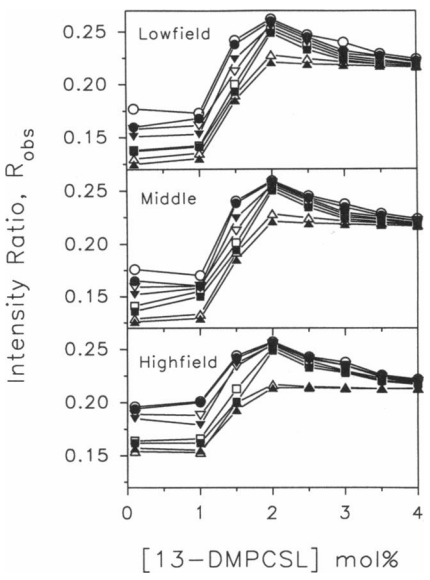

FIGURE 9 Experimentally determined intensity ratios, R_{obs}, as a function of concentration of the 13-DMPCSL spin label in equimolar mixtures of DMPC with DSPC. The upper, middle, and lower panels, respectively, correspond to the low-field, central, and high-field hyperfine lines. In each panel, data at 32 (○), 34 (●), 36 (▽), 38 (▼), 40 (□), 42 (■), 44 (△), and 46°C (▲) are shown. At 44 and 46°C the gel phase is disconnected while the fluid phase is connected. In the temperature range 32–42°C the opposite situation obtains.

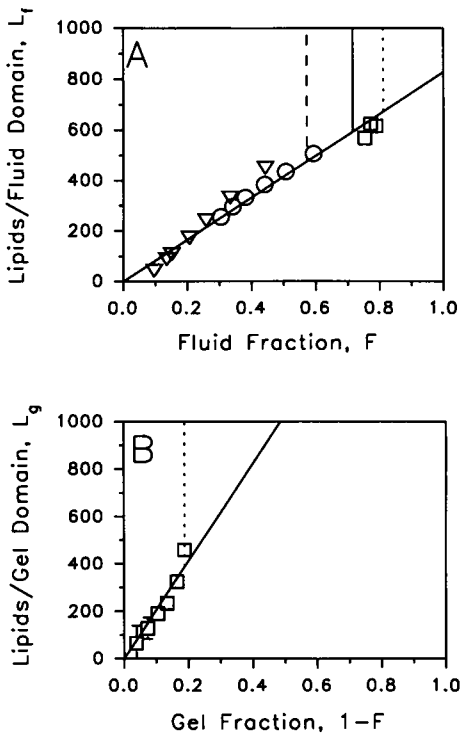

FIGURE 10 (*A*) Dependence of the average number of lipids per fluid domain, L_f, on the mole fraction, F, of lipids in the fluid phase. Data at three DMPC:DSPC mole ratios, 50:50 (○), 40:60 (▽), 75:25 (□), and different temperatures are presented. At each mole fraction of the fluid phase, the points represent averages over data obtained at 2, 2.5, 3, 3.5, and 4 mol% spin label concentrations for the low-field and central lines. The solid line is obtained by linear regression using the data for the three binary mixtures. The vertical lines represent the fluid fraction where the fluid domains for the 50:50 (*solid line*), 40:60 (*dashed lines*), and 75:25 (*dotted line*) are connected to form a continuous fluid phase. (*B*) Dependence of the average number of lipids per gel domain, L_g, on mole fraction, $1 - F$, of lipid in the gel phase. Data from the DMPC:DSPC mixture with a composition of 75:25 mol/mol (□) at various temperatures are shown. The solid line was obtained by linear regression. The vertical dotted line corresponds to the gel fraction at which the gel domains are connected to form a continuous gel phase. In both panels the error bars are standard deviations of the mean values. When the bars are not visible, they are smaller than the size of the symbols.

Fig. 10, *A* and *B*, shows the results obtained from the values of R_{obs} measured on the low-field and central lines in the ESR spectra of the 13-DMPCSL spin label incorporated at 2, 2.5, 3, 3.5, and 4 mol% in DMPC-DSPC mixtures of molar compositions 75:25, 50:50, and 40:60. The values for the size of the disconnected fluid domains are given as a function of the fraction of lipid in the fluid phase in Fig. 10 *A*, and the corresponding values for the disconnected gel phase domains are given as a function of the fraction of the lipid in the gel phase in Fig. 10 *B*. Data from the high-field line were excluded from the analysis as they did not satisfy the requirement that the

fractional linewidth changes of the component gel and fluid phase spectra be <10%.

DISCUSSION

The principal finding of this work is that lipid spin label lineshapes can be used to determine domain sizes in two-component, two-phase lipid bilayers from the statistical inhomogeneity of spin–spin interactions in the different domains. The various aspects of the study are discussed individually below, with the main emphasis being on the nucleation, growth, and nonuniform distribution of disconnected domains as determined from the dependence of domain size on the mole fraction of the disconnected phase.

Intensity ratio analysis

Conventional motional averaging analysis (Fig. 7 and Eq. 8) shows that the spin labels are not in fast exchange, on the ESR timescale, between gel and fluid phases in the coexistence region. This therefore required the development of a method for analysis of the composite lineshapes arising from spin labels in slow exchange between different domains. The intensity ratio values are shown here to differentiate diagnostically spin labels in slow exchange from those in fast exchange between two or more environments. When the spin labels exchange rapidly across isolated lipid domains, the intensity ratios will be less than or equal to the value for a Lorentzian. When the exchange rates are slow, the intensity ratios are greater than the Lorentzian value and can be used to determine the average number of spin labels per domain.

The calibrations of the average number of spin labels per domain in terms of the intensity ratio were based on a constant value for the increment in ESR linewidth per spin label per domain. This latter quantity does not remain constant in situations where the domain size changes but the total number of spin labels remains constant. However, the spectral simulations show that the intensity ratio is almost independent of this quantity in the right-hand limb of the calibration and is determined solely by the average number of spin labels per domain (see Fig. 3). Therefore, the method for determining domain size is rather robust and is relatively insensitive to the quantitative details of the line-broadening mechanism. One of the assumptions of the method is that the line-broadening in a given domain is directly proportional to the spin label concentration (cf. Eq. 3). This is certainly the case for fluid domains in which the spin–spin interactions are controlled by diffusional collisions (11, 15). In the gel phase, this proportionality is less directly established, but is likely to be approximately the case at low spin label concentration. Additionally, the method also requires that the spectra do not exhibit hyperfine anisotropy. This is demonstrated in the fluid phase, since the observed values of R are equal to those for Lorentzian lines (cf. Fig. 8). For the gel phase, small deviations are possible. The above considerations imply that the results obtained for the fluid domains will probably be more reliable than the estimates for the gel phase domains.

Domain sizes and nucleation

As seen in Fig. 10 *A*, the size of the fluid domains increases linearly with the fraction of lipid in the fluid phase. This implies that the fluid phase population increases by growth of domains, either from pre-existing nuclei or from nuclei that are formed close to the solidus boundary. New domains do not appear to be formed in appreciable numbers as the conversion to the fluid phase proceeds. Also, domains do not fuse until the system approaches close to the point of connectivity. Only then are there large upward departures from the linear dependence of domain size on fluid phase population. For the samples with mole ratios DMPC/DSPC of 40:60, 50:50, and 75:25, the linear dependence extrapolates to the origin with a gradient that corresponds to a domain density of one domain per 830 ± 20 lipid molecules. This number therefore represents the density of the initial nucleation sites.

The fact that the average domain size has approximately the same rate of growth for lipid mixtures with different compositions, although the point of connectivity occurs at quite different fractions of fluid lipid, suggests that the two-dimensional distribution of the domains must be different for mixtures of different compositions. Presumably the average center-to-center distance of the domains is smaller for the systems where the point of connectivity occurs at lower values of F, such that in all cases domains begin to collide at a point close to the respective points of connectivity. The critical domain sizes at which coalescence begins are ~350, 500, and 600 lipid molecules, which correspond to average center-to-center distances for circular domains of ~16, 19.5, and 21.5 nm for the systems with DMPC/DSPC mole ratios of 40:60, 50:50, and 75:25, respectively. For comparison, the average center-to-center distance, assuming a uniform distribution of nucleation sites with the nucleation density given above, is ~22.5 nm for a square lattice arrangement of circular domains. Thus the distribution of nucleation sites is approximately uniform for the system with a DMPC/DSPC mole ratio of 75:25 and for the other compositions the distribution is nonuniform with a preferential clustering of the nucleation sites.

The origin for the above differences in degree of fluid phase domain clustering may possibly be sought in the distribution of the immiscible gel phase components immediately below the solidus boundary (see Fig. 1). At 25 mol% DSPC composition, there is a single gel phase, Gel I. The composition of this phase is predominantly that of

the lower-melting component, DMPC. This is consistent with an approximately uniform distribution of pre-existing nucleation sites for the fluid phase. At 50 mol% DSPC, the low temperature phase is an immiscible mixture of Gel I and Gel II in roughly equal proportions, which could give rise to some nonuniformity in the pre-existing distribution of nucleation sites. At 60 mol% DSPC, the low temperature phase is also an immiscible mixture, but predominantly of Gel II, which could result in a more marked clustering of the Gel I phase that is richer in the lower-melting component and would therefore provide the fluid phase nucleation sites.

The average density of nucleation centers for the gel phase domains is considerably lower than that for the fluid phase domains. Upon extrapolation using the linear gradient, the data in Fig. 10 *B* give a domain density of one gel domain per 2,850 ± 120 lipid molecules for the 75:25 mol/mol DMPC/DSPC mixture. This is understandable because nucleation of the gel phase takes place spontaneously from the fluid phase, whereas nucleation of the fluid phase takes place from pre-existing nuclei in the gel phase. At a given fraction of the disconnected phase, the gel domains are therefore larger than the fluid domains. This also still holds for the areas of the domains after correction has been made for the different molecular areas in the two phases (cf. reference 17).

The critical gel domain size at which connectivity occurs for the 75:25 mol/mol DMPC/DSPC mixture is ~475 lipids (Fig. 10 *B*). In contrast, with the model of circular fluid phase domains on a square lattice that was applied above to the same lipid mixture, it can be estimated that the complementary gel phase domains should consist of ~270 lipid molecules at the point of connectivity. This discrepancy is partly a manifestation of the temperature dependence of R shown in Fig. 8, where it is seen that R does not go down to 0.213 and then increase again at the point of connectivity. A centered hexagonal lattice, with the center domain being gel, gives a better agreement between the gel and fluid phase data, but for a nucleation density of 1:830 lipids this predicts connectivity at a center-to-center distance of 19.5 nm. For fluid domains that are nonuniformly distributed at DMPC/DSPC mole ratios of 40:60 and 50:50, the gel phase must not automatically become disconnected at the point of connectivity.

It should be emphasized that the domain sizes determined by this method are effective average sizes; information on the heterogeneity of the size and shape of the domains is not available from these measurements. Direct imaging by electron microscopy has revealed that some domains in two-component lipid systems may have considerably larger sizes than the mean values reported here (18, 19).

Finally, the experimental effects of the connection and disconnection on a system of interacting molecules such as the spin labels discussed here are similar to those described in a recent theoretical paper. In this study the possible effects of connection and disconnection on the equilibrium configuration of a homodimerization reaction confined to one of two coexisting phases was analyzed in some detail (20). The effects on spectral lineshapes of spin label distribution in disconnected domains presented in this paper are a good approximation to the membrane-associated dimerization reaction (20).

Summaries of this work have been presented at two recent symposia (21, 22).

The expert technical assistance of Frau Gitta Angerstein in the synthesis of the spin labels is gratefully acknowledged.

This work was supported by grants GM-14628 and GM-23573 from the National Institutes of Health and by the Alexander von Humboldt Stiftung.

Received for publication 24 February 1992 and in final form 23 April 1992.

REFERENCES

1. Edidin, M. 1990. Molecular associations and membrane domains. *Curr. Top. Membr. Transp.* 36:81–96.
2. Orci, L., B. Thorens, M. Ravazzola, and H. F. Lodish. 1989. Localization of the pancreatic beta cell glucose transporter to specific plasma membrane domains. *Science (Wash. DC).* 245:295–297.
3. Rodgers, W., and M. Glaser. 1991. Characterization of lipid domains in erythrocyte membranes. *Proc. Natl. Acad. Sci. USA.* 88:1364–1368.
4. Rothberg, K. G., Y. Ying, J. F. Kolhouse, B. A. Kamen, and R. G. W. Anderson. 1990. The glycosphingolipid-linked folate receptor internalizes folate without entering the clathrin-coated pit endocytic pathway. *J. Cell Biol.* 110:637–649.
5. McConnell, H. M., L. K. Tamm, and R. M. Weis. 1984. Periodic structures in lipid monolayer phase transitions. *Proc. Natl. Acad. Sci. USA.* 81:3249–3253.
6. Nag, K., C. Boland, N. Rich, and K. M. W. Keough. 1991. Epifluorescence microscopic observation of monolayers of dipalmitoylphosphatidylcholine: dependence of domain size on compression rates. *Biochim. Biophys. Acta.* 1068:157–160.
7. Vaz, W. L. C., E. C. C. Melo, and T. E. Thompson. 1990. Fluid phase connectivity in an isomorphous, two-component, two-phase phosphatidylcholine bilayer. *Biophys. J.* 58:273–275.
8. Vaz, W. L. C., E. C. C. Melo, and T. E. Thompson. 1989. Translational diffusion and fluid domain connectivity in a two-component, two-phase phospholipid bilayer. *Biophys. J.* 56:869–876.
9. Bultmann, T., W. L. C. Vaz, E. C. C. Melo, R. B. Sisk, and T. E. Thompson. 1991. Fluid-phase connectivity and translational diffusion in a eutectic, two-component, two-phase phosphatidylcholine bilayer. *Biochemistry.* 30:5563–5579.
10. Knoll, W., K. Ibel, and E. Sackmann. 1981. Small-angle neutron scattering study of lipid phase diagrams by the contrast variation method. *Biochemistry.* 20:6379–6383.
11. Bales, B. L. 1980. A simple, accurate method of correcting for unresolved hyperfine broadening in the EPR of nitroxide spin probes to determine the intrinsic linewidth and Heisenberg spin exchange frequency. *J. Magn. Reson.* 38:193–205.
12. Bales, B. L. 1982. Correction for inhomogeneous line broadening in spin labels. II. *J. Magn. Reson.* 48:418–430.
13. Bales, B. L. 1989. Inhomogeneously broadened spin-label spectra.

In Biological Magnetic Resonance. Vol. 8. L. J. Berliner and J. Reuben, editors. Plenum Publishing Corp., New York. 77–130.

14. Marsh, D., and A. Watts. 1982. Spin labeling and lipid-protein interactions in membranes. *In* Lipid-Protein Interactions. Vol. 2. P. Jost and O. H. Griffith, editors. John Wiley & Sons, Inc., New York. 53–126.
15. Sachse, J.-H., M. D. King, and D. Marsh. 1987. ESR determination of lipid translational diffusion coefficients at low spin-label concentrations in biological membranes, using exchange broadening, exchange narrowing, and dipole-dipole interactions. *J. Magn. Reson.* 71:385–404.
16. Cevc, G., and D. Marsh. 1987. Phospholipid Bilayers: Physical Principles and Models. Wiley-Interscience, New York. 442 pp.
17. Marsh, D. 1990. Handbook of Lipid Bilayers. CRC Press, Inc., Boca Raton, FL. 387 pp.
18. Luna, E. J., and H. M. McConnell. 1978. Multiple phase equilibria in binary mixtures of phospholipids. *Biochim. Biophys. Acta.* 509:462–473.
19. Hui, S. W. 1981. Geometry of phase-separated domains in phospholipid bilayers by diffraction-contrast electron microscopy. *Biophys. J.* 34:383–395.
20. Thompson, T. E., M. B. Sankaram, and R. L. Biltonen. 1992. Biological membrane domains: functional significance. *Comm. Molec. Cell Biophys.* 8:1–15.
21. Sankaram, M. B., D. Marsh, and T. E. Thompson. 1992. Determination of average domain size in two-component two-phase lipid bilayers. *Biophys. J.* 61:A501.
22. Sankaram, M. B., D. Marsh, and T. E. Thompson. 1992. Estimation of fluid and gel domain sizes in two-component lipid bilayers. *In* Amphiphilic Membranes: Their Structure and Conformation. R. Lipowsky, editor. Springer-Verlag, New York. In press.